Simulation and Microfabrication Development of Folded-Waveguide Slow-Wave Circuit for THz Traveling-Wave Tubes

By

Ruilin Zheng

Thesis submitted in partial fulfilment of the requirements for the degree of PhD at the University of Oslo

Department of Physics

University of Oslo

June 2011

Series of dissertations submitted to the
Faculty of Mathematics and Natural Sciences, University of Oslo
No. 1126

ISSN 1501-7710

Cover: Inger Sandved Anfinsen.
Printed in Norway: AIT Oslo AS.

Produced in co-operation with Unipub.
The thesis is produced by Unipub merely in connection with the
thesis defence. Kindly direct all inquiries regarding the thesis to the copyright
holder or the unit which grants the doctorate.

ABSTRACT

Folded waveguide is considered as a robust slow-wave circuit for traveling-wave tubes, particularly for millimeter wave and terahertz wave applications. The relatively simple full-metallic structure of folded waveguide facilitates its fabrication process to be compatible with microfabrication technology, and it is structural robust and thermally stable, especially when the circuit is downsized into microscale dimensions.

In this thesis, a folded-waveguide slow-wave circuit working on 220GHz central frequency is targeted for investigation. The thesis includes two major parts, i.e. the theoretical study and electromagnetic field simulations, and an ultra-thick SU-8 process development based upon microfabrication technology.

Our cold-circuit analysis reveals that the pass-band of the 220GHz central frequency folded waveguide is ~80GHz, which is between the cut-off frequency and the first stop-band. Parametric cold-circuit study provides better knowledge about how the varying structural parameters can influence the cold-circuit parameters. Optimization of cold-circuit properties via simulation also indicates a ~20GHz 3-dB bandwidth of the circuit, and this is used as the basis of further beam interaction circuit simulations.

Following the cold-circuit analysis, we carried out the beam interaction circuit simulations and optimizations with the loss-free particle-in-cell (PIC) simulation method. Our PIC simulations reveal that the transverse dimension and shape of the electron beam tunnel have considerable impact on the beam-wave interaction. The model with circular-cross-section beam tunnel exhibits similar bandwidth, higher efficiency and gain, comparing to that with square-cross-section tunnel. It is also indicated that phase velocity taper of electromagnetic wave on the rear half of circuit can greatly improve the output power and increase the efficiency, up to 70 %. The peak loss-free output power and efficiency predicted by the PIC simulations are 70.5W and 8%, respectively.

Experimental study of microfabrication for the folded-waveguide slow-wave circuit was also conducted with the ultra-thick SU-8 process. With the help of confocal laser scanning microscopy, we quantitatively analyzed the sidewall surface roughness of the SU-8 mold.

The vertical striation along the sidewall surface was eliminated successfully by proper improvement on the post-exposure-bake conditions, and the RMS (Root Mean Square) line roughness on the SU-8 mold sidewall was greatly reduced from ~1 μm to ~70 nm. AFM analysis was also applied to examine the sidewall surface roughness, and the RMS surface roughness can be as low as 2.6 nm on the optimized samples.

A novel micromachining process for fabricating the folded waveguide was developed in our study basing on fiber embedment SU-8 process. Our preliminary results indicate that the fiber can be mounted properly in the SU-8 serpentine mold.

PREFACE

For the last four years, I have been working on the project combining two different fields, i.e. microwave electronics and microfabrication technology. I would say that the support from my family, especially from my wife Linling Yang, and advices from my supervisors, and my own hard work has brought me so far in my research work.

The works relating to my PhD research were carried out on Vestfold Universisty College, Norway, Xiamen University, China, and University of Oslo, Norway. The thesis is based on several publications and submitted manuscripts.

I would like thank my wife Linling Yang first, for her full support and understanding, and also thank my father Zhenquan Zheng and mother Qinzhu Zheng, for their continuous support of my study. I am also very grateful to my supervisors Prof. Xuyuan Chen and Prof. Per Øhlckers for their advices and inspirations. I also want to thank my colleagues Wei Sun and Lingjuan Che for their kind help during project works. I would also like to thank all the people who gave me support and help on both research and in everyday life from the abovementioned three Universities.

List of Articles

1. **Ruilin Zheng** and Xuyuan Chen, "Parametric design of microfabricated folded waveguide for millimeter wave traveling-wave tube", *Proceeding of 3rd IEEE International Conference on Nano/Micro Engineered and Molecular Systems, Jan 2008,* PP.694-699.
2. **Ruilin Zheng** and Xuyuan Chen， "Design and 3-D Simulation of Microfabricated Folded Waveguide for a 220GHz Broadband Traveling-Wave Tube Application", *Vacuum Electronics Conference, 2009. IVEC '09. IEEE International 28-30 April 2009*, Page(s):135 – 136
3. **Ruilin Zheng** and Xuyuan Chen，"Parametric Simulation and Optimization of Cold-test Properties for a 220GHz Broadband Folded Waveguide Traveling-wave Tube"，*Journal of Infrared, Millimeter and Terahertz Waves*, ISSN: 1866-6892 (Print) 1866-6906 (Online), Volume 30 number 9, pp.945-958.
4. **Ruilin Zheng** and Xuyuan Chen, "Optimization of Millimeter Wave Microfabricated Folded Waveguide Traveling-wave Tubes", *Proceedings of the 39th European Microwave Conference, 29 September - 1 October 2009, Rome, Italy,* pp. 1195-1198.
5. **Ruilin Zheng**, Haisheng San and Xuyuan Chen, "Simulation of Microfabricated Folded Waveguide Traveling-Wave Tube as Broadband Terahertz Amplifier", *Microwave Conference, 2009. APMC 2009. Asia Pacific, Digital Object Identifier: 10.1109/APMC.2009.5384471, Publication Year: 2009,* pp. 1469-1472.
6. **Ruilin Zheng**, Wei Sun, and Xuyuan Chen, “Characterizing and smoothing of striated sidewall morphology on UV-exposed thick SU-8 structures for micromachining millimeter wave circuits”, *J. Micromech. Microeng.* 20 (2010) 035007
7. **Ruilin Zheng**, Per Ohlckers, and Xuyuan Chen, “Particle-in-cell Simulation and Optimization for a 220GHz Folded-Waveguide Traveling-wave Tube”, *IEEE Transactions on Electron Devices*， Volume 58 , Issue 7, 2011, pp.2164-2171
8. **Ruilin Zheng** and Xuyuan Chen, “A Novel Approach to Micromachine Terahertz Folded-Waveguide Slow-wave Structure with Beam Tunnel of Circular Cross- section”, submitted to *J. Micromech. Microeng*

Contents

List of Abbreviations

AFM	Atomic Force Microscopy
BWO	Backward-Wave Oscillator
CLSM	Confocal Laser Scanning Microscope
CW	Continuous Wave
DFT	Discrete Fourier Transform
DRIE	Deep Reactive Ion Etching
EDM	Electric Discharge Machining
EM	Electromagnetic
HAR	High-Aspect-Ratio
HFSS	High Frequency Structure Simulator
LIGA	German acronym for Lithographie, Galvanoformung, Abformung (Lithography, Electroplating, and Molding)
MEMS	Micro-Electro-Mechanical System
OPTHER	Optically Driven Terahertz Amplifiers
PEB	Post-Exposure Bake
PGA	Photon Generated Acid
PIC	Particle-In-Cell
PMMA	PolymethylMethacrylate
PPM	Permanent Periodic Magnet
QCL	Quantum Cascade Laser
RMS	Root Mean Square
SOI	Silicon-On-Insulator
SWS	Slow-Wave Structure
TWT	Traveling-Wave Tube
UV	Ultra-Violet

1 Introduction

1.1 The Terahertz Gap and Terahertz Applications

Sandwiched between microwave band and infrared (IR) band, the terahertz wave band (defined as 100GHz-10THz here) still remains one of the least exploited regions of the electromagnetic spectrum [1-3]. This bandgap region, as shown in fig.1.1, is out of reach for the usual optical and electronic measurement techniques normally related to these better-known neighbours [1, 4]. Despite great scientific interest since at least the 1920s, the absence of compact, powerful and low-cost THz sources and relative sensitive detectors working within the THz region made THz band an insurmountable gap between the traditional microwave and optical technology for decades [1-3]. The under-developed THz technology and its very promising potentials for applications makes this region of the electromagnetic spectrum a scientific frontier, and a lot of research efforts have been attracted to the terahertz field in the recent years.

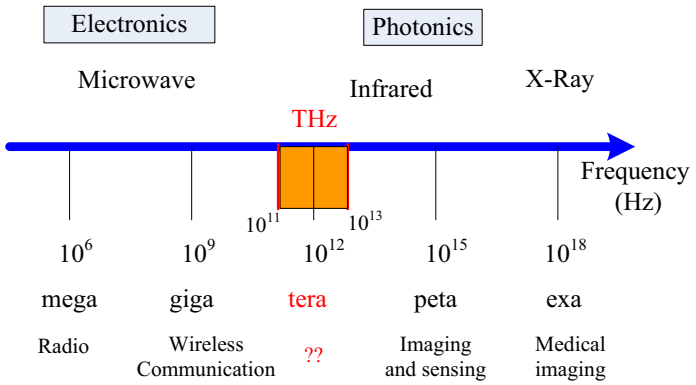

Figure 1.1 The electromagnetic spectra showing the THz bandgap between microwave band and infrared band.

The promising applications of the THz technology fall into several categories as follows: THz imaging, THz radar, THz spectroscopy and THz wireless

communication [1-6]. The ability of THz wave to penetrate some materials that are usually opaque to both visible and infrared radiation attracts a lot of research interests. Many potential applications of THz imaging in medical care are being exploited, for example non-invasive inspections for diagnosis of skin cancer and breast cancer, as the THz radiation has much lower radioactive energy comparing to X-ray radiation which can cause ionization. THz technology also has promising prospects in homeland security applications. For instance, surveillance systems based upon THz imaging techniques can detect hazardous material hidden in envelopes, or weapon concealed behind terrorists' clothes when they are passing a security checkpoint. THz radar can be employed to detect targets through fog over hundreds-meters distance on the battle field as well. Within the communication area, broadband THz sources and amplifiers are the prerequisite to realize ultra-high-data-rate wireless communication. For example, 10% of bandwidth of a 400GHz central frequency can enable wireless transmission at a data rate higher than 100Gbps. The security of wireless and inter-satellite communications can also benefit from the miniaturized antenna, as it can produce highly directional beam. As THz fields interact strongly with polar substances but penetrate those non-polar ones, the absorption spectra of many polar molecules, for example H_2O, C, N_2, O_2, O_3, HCl, CO, SO_2, CH_3CN, etc., have many and distinct spectral peaks in the THz range [2]. This unique signature of molecules in the THz range is of significant importance in monitoring the surrounding medium, air pollution detection, or gas sensing [2-4, 7, 8]. Since various interesting materials have unique fingerprints in the THz range, it means that THz radiation can be used to identify specific materials. Because many materials are transparent to THz and THz radiation is non-ionizing, and images formed with THz radiation can have relatively high resolution, we can employ THz spectroscopy as a non-destructive method for analyzing materials.

As aforementioned, the bottle-neck of applying THz technology is the lack of compact and reliable terahertz sources with considerable output power and low cost. Only some very bulky and expensive sources, such as IR-pumped gas laser, free electron laser, backward-wave oscillator (BWO) and THz quantum cascade laser

(QCL), can generate output power over 1mW at around 1THz [1, 2, 4]. The lack of suitable THz sources is strongly inhibiting the development and future applications of THz technology.

To develop compact and powerful terahertz sources and amplifiers, currently there seems to be two possible choices, either extending the operating frequency of current electronic devices upwards from the microwave band or extending the operating frequency of present photonic devices downwards from the IR band into the THz range. Analogous to the semiconductor laser diode in the visible and infrared band, or to the transistor oscillators and amplifiers in the microwave frequency band, a compact, coherent and continuous wave (CW) THz solid-state source is strongly desirable for THz systems. However, the power generated by solid-state electronic devices, such as transistors, Gunn oscillators and Schottky diode multipliers, rolls off owing to both transit-time and resistance–capacitance effects when working frequency rises into the low frequency end of the THz range [1, 5]. The direct generation of THz wave through photonic approach is hindered by the lack of appropriate materials, which should have sufficient small band-gap for radiating THz waves [4]. Although intersubband QCL with atomically sharp semiconductor heterostructures, powered by the advance of nanotechnology, is capable for generating both pulsed and CW radiation of hundreds of mWs at the frequency rang around 1THz. However, the requirement of cryogenic working environment is definitely a huge drawback of this technology [3-5]. Nonlinear photo mixing of two laser sources is an alternative optical approach for indirectly generating THz wave, but this technique suffers from the very low conversion efficiency, low output power and bulky equipment [4, 9].

There is a promising approach to achieve compact THz sources through increasing the working frequency from microwave band into the THz frequency range for the present microwave tubes (or electron tubes), which can provide much higher output power and broader bandwidth than solid-state devices [6, 10-12]. Nonetheless, the physical scaling problem and the metallic loss issue are obstacles preventing microwave tubes devices from working in the THz frequency range [1, 2, 11]. To address these problems, miniaturization of electron tubes with microfabrication

technology is introduced as a reasonable approach [6, 12, 67, 68]. Recent technological advance in microfabrication and development of micro-BWO have reflected the powerful capability of THz electron-tube devices and revealed their promising prospects [13, 70].

1.2 Traveling-wave Tubes and Their THz Version

Among the family of microwave tubes, traveling-wave tubes (TWTs) occupy more than 50% of the market share. Generally, TWTs can work as high gain and broadband amplifiers, as well as oscillator when a feedback loop is applied [14-16]. TWTs are found in almost every communication satellite as final stage amplifiers. In many radar systems, one or more TWTs are used as high power amplifier to generate the transmitted RF pulse. The largest application of TWTs is in electronic

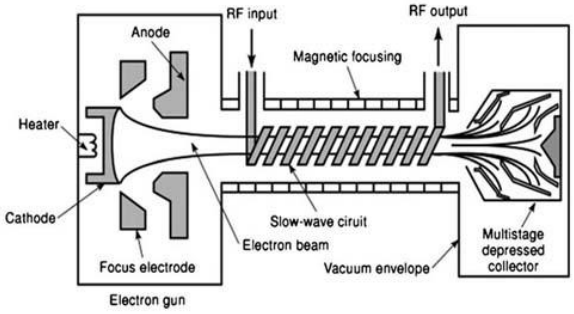

Figure 1.2 A schematic configuration of helix-TWT

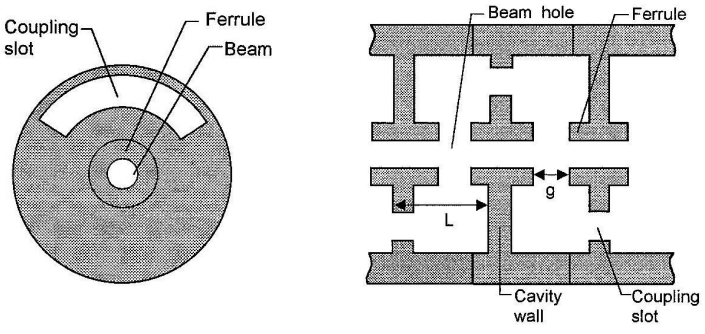

Figure 1.3 (a) End view and (b) cross-section view of coupled-cavity slow-wave circuit.

countermeasure systems, in which TWTs serve as power amplifiers for transmitting deceptive signals [14]. Other applications of TWTs include key amplifiers in remote sensing system and wireless communication systems, for example terrestrial microwave communication [10, 11].

For their indispensable importance in the vacuum electronics devices, the development of miniaturized THz TWTs draws a lot of attentions from the vacuum electronics community [17-24]. Developing a THz TWT means that almost every part of TWT need to be miniaturized accordingly since the transverse size of circuits is inversely proportional to the working frequency. Fig.1.2 shows a typical configuration of a helix-TWT, which consists of a thermionic electron gun, a wounding helix slow-wave circuit, input/output coupler for signal, external magnet for focusing the electron beam and a depressed collector to gather the used electron beam. The working principle of a TWT is to transfer the kinetic energy of electron beam to the electromagnetic (EM) field energy along the slow-wave circuit as continuous beam-wave interaction takes place under the condition that the axial phase velocity of EM wave matches the speed of the electrons drifting inside the tube [14]. As a result, RF signal is amplified. Since it is impossible to accelerate electron to the speed of light in vacuum, a slow-wave circuit is applied to slow down the axial phase velocity of EM wave, in order to match the speed of electron beam [14-15]. At present, helix and couple-cavity (see fig.1.3) are the two most widely used types of slow-wave circuits for microwave band TWTs. Working as the interaction circuit for TWTs, slow-wave circuit determines the gain, power capability and bandwidth of TWTs [25, 26]. For example, a TWT with helix as the slow-wave circuit is capable for providing very broad bandwidth (>30% of the central frequency) but relatively low output power [10]. On the other hand, a couple-cavity TWT can produce higher gain and output power than the helix-TWT but the bandwidth is much narrower (<20% of the central frequency). In the past decades, some novel slow-wave circuits have also been designed and developed for TWTs in the millimetre and sub-millimetre wave bands[30, 32, 49, 50- 52, 71-72].

Table 1-1 Microfabricated slow-wave circuits for TWTs

Group	SWS	E-beam	Frequency	Saturated output/ bandwidth	Process
University of Wisconsin-Madison	Folded waveguide	Pencil beam	560GHz	>70mW ~60GHz	X-ray and UV-LIGA, DRIE
Northrop Grumman	5-way combined folded waveguide	5-way pencil beam	220GHz	>10W ~20GHz	UV-LIGA, DRIE
University of California-Davis	Staggered double vane	Sheet beam	220GHz	>100W ~50GHz	UV-LIGA
Teraphysics Corporation	Helix	External, half-ring cross-section	650GHz	270mW/ NA	Bulk and surface micromachining
National Seoul University	Folded waveguide, coupled-cavity	Pencil beam	100GHz	NA	2-step X-ray LIGA
OPTHER, Europe	Corrugated waveguide	Sheet beam/pencil beam	0.3-2THz	10-100mW	UV-LIGA

Because the slow-wave circuit is such a key part of a TWT, plenty of works on miniaturizing TWTs are focusing on achieving downsized slow-wave circuits [10]. Concerning the fabrication issue of slow-wave circuit for THz TWTs, the main problems are the very stringent machining tolerance required by the miniaturization of slow-wave circuit and demanding control of the surface roughness of metal for reducing the resistive loss due to the decreasing skin depth of metal under very high frequencies [6, 27, 47, 48]. Apparently, conventional machining techniques are not suitable for very demanding tolerances, for instance the requirement of machining tolerance around 1μm and the sidewall RMS (Root Mean Square) surface roughness around hundred nanometres, are far beyond the levels that the conventional machining

techniques can reach. Furthermore, the traditional helix and couple-cavity slow-wave circuits are difficult to fabricate with micromachining technique, owing to their rather complex structures. Therefore, both new type of slow-wave circuits and relating microfabrication technologies are required to develop THz TWTs.

In the past decade, several types of microfabricated slow-wave circuits have been proposed for THz TWTs, such as folded waveguide [18-20, 54-56, 64, 70], corrugated waveguide [23, 71-72] and staggered vane structure [21, 22, 73,74]. Some researchers are also making efforts on the modified helix [24] and coupled-cavities slow-wave circuits [29]. Table 1-1 lists out some details about the projects relating to the microfabricated THz TWTs carried out by different groups across the world. Some of these slow-wave circuits have demanding requirements for the electron beam. For example, as shown in table 1-1, both staggered double vane and corrugated waveguide structures may require an electron sheet beam to drive the devices, while the miniaturized modified helix structure needs external electron beams which have half-ring-shape cross-section to drift outside the helix [71, 21, 28]. The complexity

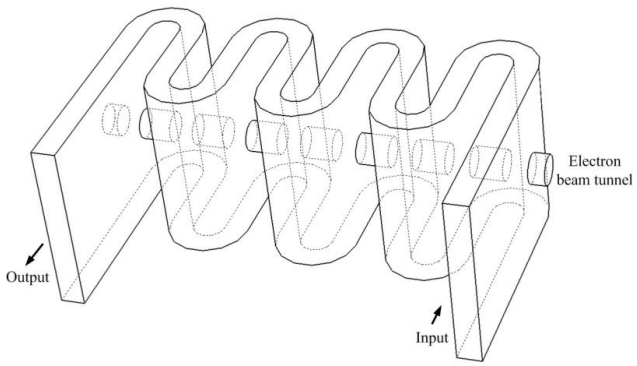

Figure 1.4 Three-dimension model of hollow folded waveguide structure

arising from electron beams will greatly increase the difficulty for implementing miniaturized THz TWTs.

As for folded-waveguide slow-wave circuit, it needs only a pencil-shape electron beam to drive the circuit, which is much easier to obtain. A 3-dimension (3-D) model of a hollow folded waveguide is shown in fig.1.4. The performances of folded

waveguides are compromises between those of helix and coupled-cavity slow-wave circuits [26]. Proven by the experiment, folded-waveguide slow-wave circuits have the merits of relatively broad bandwidth, moderate output power and low RF loss within the millimetre wave range [26, 30, 66]. The relative simple and full-metal structures of folded waveguides also guarantee better compatibility with microfabrication technology, higher thermal capability and higher reliability of device. This makes folded waveguide more competitive when the circuit is downsized to accommodate increased frequencies.

1.3 Research on Folded-Waveguide Slow-Wave Circuit

Folded waveguide has been studied as slow-wave circuit of the TWT for over two decades since Doher et al. made the first experimental folded-waveguide TWT working at 45GHz [30]. Linear theory and equivalent circuit analysis of the folded-waveguide slow-wave circuit was introduced by Ha et al. in 1998 [44]. Based on analytical study, equivalent circuit model and electromagnetic field simulation, Booske et al. presented their modeling method for folded-waveguide slow-wave circuit with better accuracy [34]. The author also conducted parametric analysis on the folded-waveguide slow-wave circuit with regard to the structural parameters and provided optimization method via parametric study and electromagnetic field simulation [36]. In his publication, Malek presented that the analytical results obtained with Madey's theorem, instead of the widely used Pierce theory, agree very well with the numerical results obtained by Matlab program using single particle under small signal gain condition [53]. However, Malek's simplified results have not been compared with electromagnetic field simulations for verification yet [53]. Experimental studies on folded-waveguide TWT are also conducted within millimeter wave range and THz wave rage for high power application [65, 66,70].

Towards enhancing performance of folded-waveguide slow-wave circuit, such as gain, power level and bandwidth, substantial research activities are focusing on the

structural modifications of the full-metal folded waveguide. For example, Northrop Grumman is developing parallel folded waveguides instead of a single waveguide, in order to boost the power level of folded-waveguide TWTs [20, 54-56]. Some theoretical analyses have been focused on adding specific parts onto the normal folded-waveguide structure. For instance, He et al. [52, 57] and Sumathy et al. [58] presented their analysis on ridge-loaded folded-waveguide slow-wave circuit, respectively, to widen the bandwidth of folded-waveguide TWT. Dielectric-loaded folded waveguide was studied by Zhang et al., in order to broaden the bandwidth for the millimeter TWTs [59]. Resonance-cavity-like structure added to the normal folded-waveguide structure was investigated for the purpose of increasing beam-wave interaction capability, which is reported by Liao et al in their simulated results [60-61]. However, this modification causes a smaller bandwidth [62]. Though structural modification sounds as a good idea to improve specific properties of the folded-waveguide slow-wave circuit to a certain degree, the fabrication challenges for the microfabrication technology are also increased. Hence there will be a long way to go before these modified folded-waveguide structures can be realized.

To improve the efficiency of folded-waveguide slow-wave circuit, non-uniform periods of the folded waveguide, or electromagnetic wave phase velocity tapering near the output end of folded waveguide, are applied to resynchronize electron beam and the electromagnetic wave and extract more kinetic energy from electron beam to the wave [63].

In recent decade, we can see that more and more research interests in folded-waveguide slow-wave circuit are moving into the region of THz [67-70], due to its promising properties and compatibility with mature microfabrication technology. We will discuss about this in next section.

1.4 Microfabricated THz Folded-Waveguide Slow-wave Circuit

Since the first time Kory et al. proposed the idea of microfabricated

folded-waveguide slow-wave circuit for THz TWT and BWO applications, many research efforts have been done on the development of micromachining processes for miniaturized folded-waveguide circuits [16]. Two typical high-aspect-ratio-structure (HARS) micromachining techniques, i.e. DRIE (Deep Reactive Ion Etching) and LIGA (German acronym of “Lithographie, Galvanoformung und Abformung", means lithography, galvanoforming and molding), have been applied for fabricating the prototypes of folded-waveguide slow-wave circuit [6, 18, 20, 32, 76]. DRIE uses silicon wafer or SOI (Silicon-On-Insulator) wafer as substrate, and creates the structure on the wafer in a substractive way, i.e. etching away the silicon [31]. While for LIGA, a substrate with conductive seed layer is required, i.e. metallic wafer or silicon wafer coated with metallic layer. The LIGA-fabricated structure is created in an additive way, i.e. electroplating metal onto the sacrificial structure of photoreisit [31]. Both DRIE and LIGA are able to create structure with considerably smooth sidewalls [77-78].

Micro-EDM (Electrical Discharging Machining) has also been used to machine W-band (83.5GHz) folded–waveguide slow-wave circuit [6]. However, Micro-EDM is no longer suitable when both very high machining accuracy and very smooth surface (RMS roughness less than a hundred nm) are required, thus it is not suitable for THz circuit microfabrication. Therefore photolithography-based microfabrication processes, like DRIE and LIGA are the preferable approaches for micromachining of THZ folded-waveguide circuits.

Because folded-waveguide circuit has an electron beam tunnel longitudinally across the entire serpentine waveguide structure (see fig.1.4) and the beam hole exists in the middle of the serpentine waveguide sidewall if we look at the cross-section, this difference in cross-section size for the beam tunnel and the serpentine waveguide complicates the microfabrication process with additional steps and increasing micromachining errors. Much more effort is required for fabricating the electron beam tunnel. In order to machine the electron beam tunnel, in general, folded waveguide is divided into two symmetric halves and each part is fabricated individually. Each symmetric part of beam tunnel should be structured in a different step apart from the

step for creating serpentine waveguide, before the two symmetric halves of folded waveguide are aligned and assembled together. Taking LIGA process for example, at first, one half of the serpentine hollow waveguide is created through electroplating of copper onto the lithographically patterned polymethylmethacrylate (PMMA) photoresist and release of the photoresist; then the semi-circular-column-shape or rectangular-column-shape half of the electron beam tunnel is trenched on the LIGA-fabricated copper waveguide with micro-EDM; and at last the two symmetric halves are assembled together. Although micro-EDM process might be a very reasonable approach to create long trench for the beam tunnel of a folded waveguide, the process does trigger new problems. In [32], Shin et al. reported that the hollow serpentine waveguide as EM wavepath would be clogged and distorted by the burs generated in the micro-EDM process, which tear the copper off the LIGA-fabricated block, as shown in fig.1.5(a). To address this problem, they developed a new two-step LIGA process for machining, in which the serpentine waveguide and rectangular-column-shape electron beam tunnel are fabricated in individual steps and additional alignment is involved [32]. Their sample of two-step LIGA process is shown in fig.1.5(b).

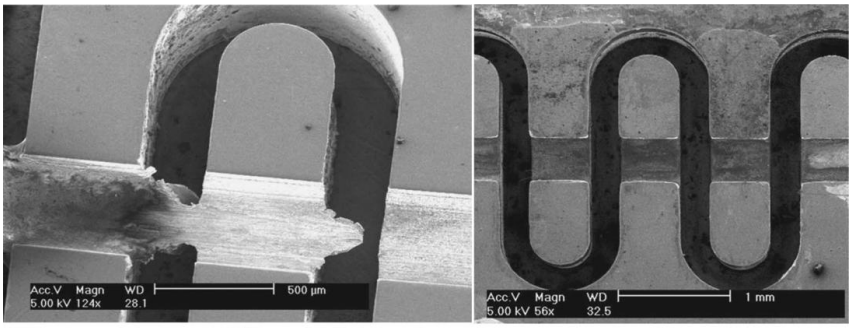

Figure 1.5 (a) X-ray LIGA fabricated folded waveguide with beam tunnel machined by EDM and (b) two-step LIGA fabricated folded waveguide.

Standard LIGA is a very robust technique for fabricating microstructures with HAR, because it applies a coherent X-ray as exposure source, which has low

dispersion. However, employing standard LIGA requires very expensive coherent X-ray source, i.e. synchrotron, which is usually unaffordable for most laboratories, and this strongly limits the application of LIGA. DRIE can be widely accessed though it is an expensive technique as well. The major challenge with DRIE for machining folded-waveguide is how to control the sidewall roughness of the structures.

To replace the very expensive X-ray as the exposure source for micromachining HARS, widely deployed ultraviolet (UV) exposure source is employed in a modified LIGA process. As the PMMA used in standard LIGA process requires very high exposure energy to break the link, which is not suitable for UV process. A new negative tone ultraviolet (UV) sensitive photoresist, i.e. SU-8, is an alternative for micromachining HARS [6, 31, 33, 41]. The SU-8 based UV-LIGA process is more accessible as UV exposure source is affordable to every MEMS lab. Nowadays, SU-8 has been employed to fabricate the mold for folded waveguide. Fig.1.6 shows an SU-8 mold of folded-waveguide structure for 400GHz TWT fabricated by Booske et al. [6, 19]

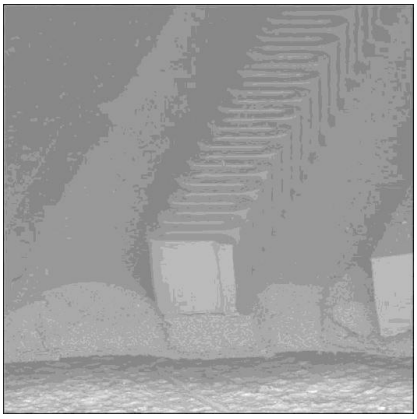

Figure 1.6 SU-8 mold of folded waveguide for 400GHz application

Both LIGA and UV-LIGA are merely capable for quasi-3D microfabrication of structures, owing to the limitation of photolithography, which in principle only can transfer 2-dimension pattern from the photomask onto the photoresist [31, 33]. As well, DRIE can only etch along Z direction and the XY-plane cross-section remains unchanged, if the mask is set in XY plane, which means only quasi-3D structure can

be fabricated from 2D mask [31]. As a consequence, the electron beam tunnel fabricated by these techniques should have a rectangular or square cross-section. The drawback of rectangular-column-shape electron beam tunnel is that the circuit has lower beam-wave interaction, and lower efficiency than the beam tunnel of circular cross-section when applying pencil-shape electron beam. Additional alignment may also introduce more machining errors in the process.

A lot of research efforts are also focused on the theoretical analysis and EM field simulation of THz folded-waveguide slow-wave circuit [34-40]. Accurate analysis on folded–waveguide slow-wave circuits is important for the design of TWTs. The design process can be greatly accelerated and the design cost can be cut by means of accurate analysis and simulation since prototyping of the device is not necessary and the risk of design failure can be reduced [42]. The theoretical analysis on slow-wave circuit falls into two categories, i.e. cold-circuit (or cold-test) in which the real electron beam is not taken into account, and beam-interaction circuit (or hot-test) analysis, in which the real electron beam is taken into account [42, 43]. Cold-circuit analysis focuses on the dispersion relation and the beam-wave interaction impedance, and the circuit loss of the cold-circuit [42-44]. Beam-interaction circuit analysis usually bases on the results obtained from cold-circuit analysis, and takes the real electron beam into account, when calculating the amplifier characteristics, such as bandwidth, gain and output power.

Generally, cold-circuit analysis of folded-waveguide slow-wave circuit consists of three major methods, i.e. analytical model, equivalent circuit model and EM field simulations [34, 44]. Analytical model describes the dispersion relation in a simplified way since the calculations of axial phase velocity of EM wave and the electric field are performed ignoring the bending of the waveguide and the beam hole on the broad wall of the waveguide [34, 44]. Based on waveguide theory, equivalent circuit model employs different circuit models, to represent each part of the folded waveguide, i.e. the bending part and the straight part of waveguide, the junction between bending and straight part and the beam hole on the broad wall. Then the dispersion relation and electric field can be calculated [44]. EM field simulations apply FEM (Finite Element

Method) or FIM (Finite Integration Method) to calculate the EM field within the entire meshed folded-waveguide structure [34].

In general, the design flow starts with cold-circuit characteristics, by building up analytical model and equivalent circuit model, and running eigenmode EM filed simulation. Then the beam-interaction circuit simulation can be carried out based on the parameters achieved in cold-circuit analysis, by means of particle-in-cell (PIC) simulation program. Circuit optimization can also be carried out with both cold-circuit and beam-interaction circuit simulations.

Within a slow-wave circuit, the EM field is determined by Maxwell's equations with source current and charge density, while the electrons are governed by the Newton's law or their relativistic version [16, 42]. These equations are coupled together in the way that the EM field is induced by the current and charges of the moving electrons, while the electrons move according to the EM fields [14-16, 42]. The most accurate way to obtain solutions for the Maxwell-Newton's system of equations, is to directly solve them. To provide self-consistent solutions for the governing equations, the PIC method was developed [42]. In the PIC method, the arbitrary functions of charged particles are statically represented with discrete computer particles, and the computer particles exist in a continuum space and interact with EM fields through a discrete grid using interpolation [42]. However, the calculations with the PIC method are much more complicated and time-assuming, due to the complexity of solving self-consistent equations and tedious interpolation process. With the advance of computing power of modern computer and the advent of commercial simulator, the PIC simulation has become realistic and the computing challenge is reduced remarkably.

Most of the verifications of circuit designs for THz folded-waveguide slow-wave circuits are still limited in testing the cold-circuit properties for the circuits fabricated, or building-up lower-frequency scaled device and testing the amplifier performance [19, 20, 32]. By now, we have only found experimental work related to THz folded-waveguide TWT in one paper [70].

1.5 Research Goals and Approaches

We aimed at developing folded-waveguide slow-wave circuit with relatively broad bandwidth and high output power for 220GHz central frequency TWT. The designed bandwidth is about 20GHz, and the expected output power of the continuous wave is around 10W. Powerful broadband amplifier working around the 220GHz atmospheric window will enable plenty of applications, such as short range THz radar system for homeland security uses and military uses, remote sensing system for commercial, academic and military applications and ultra-high-data-rate wireless communications (>60Gbps) and inter-satellite communications.

Our research effort covers the microwave theoretical study, electromagnetic field simulations and the microfabrication technology together. We apply the microwave electronics theory and powerful numeric computing tools to build up folded-waveguide circuit models, parametrically analyze the structures and carry out the optimization for circuit properties. Another part of effort is developing new micromachining process for folded-waveguide slow-wave circuits. We chose to use the SU-8 based UV-LIGA-like process to realize our design. The critical process steps were developed for specific parameters, such as the side wall surface smoothness and circular cross-section beam tunnel.

1.6 Thesis Outline

This thesis focuses on the design, parametric simulation and optimization of folded-waveguide slow-wave circuit with 3-D EM simulator, and development of relating microfabrication technology. The structure of the thesis is based on the published and submitted journal articles. First part of the thesis is the introduction of research background. The following two parts describe the methods involved in the research works. In the second part, the design process, the analytical and numerical analyses of the folded-waveguide slow-wave circuit are presented. Both cold-circuit and beam-wave interaction analyses are made on EM field simulations. Analytical

model, equivalent circuit model and high frequency structure simulator (HFSS) models, as well as the detail parametric analysis and optimization on cold-circuit properties, are included in the cold-circuit studies of folded-waveguide circuit. Our beam-wave interaction analysis puts emphasis on the 3-D time domain particle-in-cell simulation with CST particle studio, in which the amplifier characteristics of folded-waveguide TWT are verified and optimized. The third part presents the experimental studies on the SU-8-based microfabrication process for folded waveguides. A striated sidewall surface morphology on the ultra-thick SU-8 structure was analyzed in detail, and a method to optimize the process and smooth the sidewall is also introduced. A novel microfabrication process for folded waveguides was proposed, in which the optical fiber is embedded as a sacrificial structure for machining the centimetres-long beam tunnel of circular cross-section for the folded waveguide. The last part gives the summaries of the published and submitted articles, and presents the major results and conclusions. The articles are attached at the end of the thesis, and the more specific results and discussions of each article are given.

2 Electromagnetic Field Simulation and Optimization for Folded-Waveguide Slow-Wave Circuit

To facilitate and accelerate the design process, to reduce the risk and cost of development, and to optimize the performance are always the goals to achieve when designing traveling-wave tubes (TWTs). Nowadays, electromagnetic (EM) field simulation as a powerful numerical method is indispensable for designing TWTs and predicting the performance of the designed devices [11, 42]. Benefiting from the ever-advancing modern computing technology, the EM field simulation becomes more and more accurate and efficient for modeling TWTs, and plays more and more important role on the design process of TWTs.

In this part, the methods to design the slow-wave circuit, and how to model the folded-waveguide circuit and optimize the amplifier characteristics are introduced. Usually, the design flow starts with the cold-circuit design and modeling, i.e. without considering the influence of the electron beam. After obtaining basic structural parameters and preliminary results via cold-circuit modeling, the beam-wave interaction modeling, i.e. taking into account the electron beam, is carried out to further simulate, analyze and optimize the design. Both cold-circuit design and modeling, and the beam-wave interaction modeling are presented here.

2.1 Cold-circuit modeling and parametric simulation

As a preliminary step to design a TWT, the cold-circuit properties of folded-waveguide circuit should be analyzed and optimized with the structural parameters. The cold-circuit properties here refer to phase velocity of electromagnetic

wave propagating in folded waveguide, the on-axis beam-wave interaction impedance K_c and circuit attenuation, with the absence of a real electron beam. The cold-circuit parametric simulations of folded waveguide were conducted in one pitch (half period) circuit with a high frequency structure simulator (HFSS), assisted by analytical model and equivalent circuit model. To provide a basis for circuit optimization, parametric simulations are used to find out how the structural parameters influence the cold-circuit properties of the folded waveguide. The circuit attenuation per pitch, due to conduction loss, was also calculated from the HFSS simulated 3-D electromagnetic field distribution.

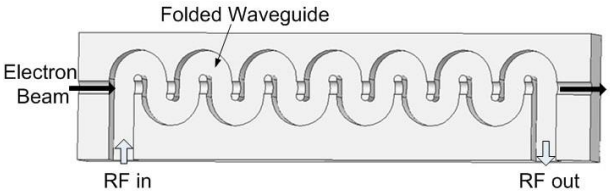

Figure 2.1 Three-dimension cross-section structure and brief function of folded waveguide

The cross section of a folded waveguide is shown in fig.2.1. It includes a serpentine waveguide for traveling wave to slow down its phase velocity to the speed of electron drifting inside the electron beam tunnel, and input/output coupler for RF signal going in and out. The material for the folded waveguide should have high electrical and thermal conductivity, and copper is our best choice. In the following paragraphs, analytical model, equivalent circuit model and HFSS simulation methods are presented. The methods for calculating phase velocity, beam-wave interaction impedance and circuit attenuation are also given.

2.1.1 Analytical model

Based on published results from other researchers [30, 44, 81], the ratio of central frequency to the cutoff frequency is assigned to be 1.25, hence the width of the transverse rectangular waveguide '*a*' is fixed to be 0.852mm for the TE_{10} mode in the

220 GHz folded-waveguide slow-wave circuit. The parametric simulations were conducted with the rest of major structural parameters, as displayed in fig.2. 2(a).

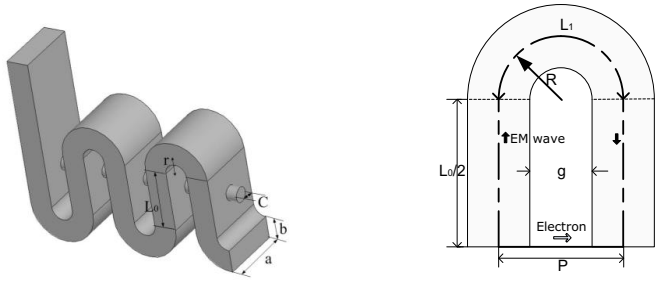

(a) (b)

Figure 2.2 (a) 3-D structure and (b) 2-D sketch map of folded waveguide circuit. The width and height of the transverse rectangular waveguide are *a* and *b* respectively. Parameters *D*, *r* and *g* are the diameter of electron beam tunnel, mean radius of E-plane bending and gap between two adjacent straight waveguide, respectively. *P* is on-axis length of one pitch (half period).

Since a folded waveguide is a periodic structure, the circuit parameters can be tested only within one pitch. The analytical model of a folded waveguide is illustrated in fig.2.2 (b). The E-plane bending waveguide is treated as straight waveguide. Thereby, the electromagnetic wave path L is defined as the sum of straight-waveguide-length L_0 and mean length of E-plane bending L_1, in one pitch. The influence of the beam tunnel is not considered in this analytical model. As the analytical model neglects the bending of the waveguide and the electron beam hole on the broad wall of the straight part of the folded waveguide, it is considered as simplified circuit model. The phase delay θ per pitch of the EM wave obtained in the analytical model is,

$$\theta = 2\pi L/\lambda_g = (2\pi Lf/c)\sqrt{1-(\frac{f_c}{f})^2}, \lambda_g = \lambda/\sqrt{1-(\frac{\lambda}{\lambda_c})^2} \quad (2\text{-}1)$$

where λ_g and λ_c are waveguide wavelength and cut-off wavelength respectively, and c is the velocity of light in vacuum.

2.1.2 Equivalent-circuit modeling

According to transmission line theory, a folded waveguide can be modeled with a circuit, and different parts of folded waveguide can be described with different components，which have their own transmission line transfer matrix [34, 44, 79]. As shown in fig.2.3, the waveguide is divided into three parts: The electron beam hole, the straight waveguide and the E-plane bending waveguide.

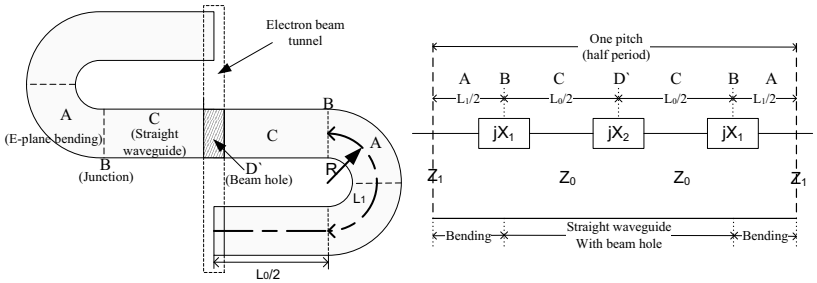

(a) (b)

Figure 2.3 (a) Divided parts and (b) equivalent circuit model of folded waveguide.

The straight waveguide is treated as a uniform transmission line with characteristic impedance of Z_0. The E-plane bending is a uniform circular bend of a rectangular waveguide, and it is here considered to have a characteristic impedance of Z_1. The junction between the straight and bending waveguides and the beam hole on the straight waveguide are represented by two different reactances X_1 and X_2, respectively. The single transmission line transfer matrix F for one pitch of the circuit can be obtained by calculating cascaded transfer matrices of these components in serial [34, 44]. Finally, a dispersion equation for the folded waveguide is achieved, which will provide the basis for phase velocity and interaction impedance calculations. With E-plane bending and beam hole taken into account, an equivalent-circuit model has higher reliability than an analytical model as representing cold-circuit properties for folded waveguides. The detailed introduction of equivalent circuit model for folded waveguides was included in references [34, 44]. The equivalent-circuit modeling method is employed to assist the analyses process here.

2.1.3 HFSS simulation

Based on the calculated results of analytical and equivalent-circuit analyses, the EM field simulations with HFSS were carried out on the folded-waveguide circuit. The Ansoft HFSS is a powerful program in 3-D electromagnetic field simulation for passive devices. Being able to mesh the arbitrary-shape structure into hundreds of thousands of tiny cells, and calculate the Maxwell's equations directly inside each cell, HFSS can achieve much better accuracy than analytical models and equivalent circuit models. By employing adaptive meshing, volume perturbation technique and periodic boundary in the eigenmode solver of HFSS, folded waveguide circuits can be simulated accurately and efficiently within a pitch. Based on the simulated resonant frequency at specified phase delay and 3-D electromagnetic field distribution, the cold-circuit properties can be calculated in the post-processing step. Through parametric simulations, we analyzed how the varying structural parameters alter the circuit properties, and further optimized the cold-circuit performance basing on the parametric results.

2.1.4 Calculation of the cold-circuit properties

Normalized phase velocity of the 0^{th} spatial harmonics of TE_{10} wave is defined as angular frequency divided by the product of vacuum light speed and propagation constant, as shown in eq. 2-2.

$$v_{phm} = \frac{\omega}{c\beta_m} = \frac{(\theta + \pi)}{c\beta_m} \qquad (2\text{-}2)$$

For an equivalent circuit model, the phase shift over one pitch is calculated with the dispersion equation at given frequency, and plus 1 π as for the 0^{th} spatial harmonics. For HFSS simulation, the resonant frequency is the simulated eigenfrequency and the corresponding phase shift is the sum of given phase delay and 1π.

The electron beam is assumed to interact with the on-axis axial part of electric field, generally. The interaction impedance depicts how much on-axis axial electric field is

available for a given power propagating down the circuit, defined as below, assuming electron beam propagating along the z axis:

$$K_{cm} = \frac{|E_{zm}|^2}{2\beta_{zm}^2 P_{wg}} \tag{2-3}$$

where K_{cm}, E_{zm} and β_{zm} represent the interaction impedance, the on-axis axial electric field and propagation constant of the mth spatial harmonics, respectively, and P_{wg} is the time-average power propagating down the waveguide [16, 82].

In the post-processing step of HFSS simulation, E_{zm} is obtained by spatial Fourier analysis across the on-axis pitch length and the loss-free P_{wg} is computed by integrating the Poynting vector across the transverse section of the folded waveguide, as given in eq.2-4.

$$P_{wg} = \frac{1}{2}\int_{-a/2}^{a/2} dx \int_{-b/2}^{b/2} \vec{E} \times \vec{H}^* \, dy \tag{2-4}$$

The attenuation of the cold circuit per pitch due to resistive loss of conductor is computed with the perturbation method introduced in Pozar's book [80], as defined in eq.2-5:

$$\alpha_{pitch} = \frac{P_{cl}}{2P_{wg}} \tag{2-5}$$

where P_{cl} represents the power absorbed by the conductive wall of the folded waveguide in one pitch length, while loss-free P_{wg} is defined in eq.2-4. P_{cl} is given as below:

$$P_{cl} = \frac{R_s}{2}\int_s |H_{tan}|^2 \, ds \text{, where } R_s = \sqrt{\frac{\omega\mu}{2\sigma}} \tag{2-6}$$

R_s, σ and μ are the surface resistivity, bulk conductivity and the permeability of the conductor, respectively, H_{tan} is the magnetic field intensity tangential to the waveguide surface, and the s in the integral represents the inner conductive surface of folded waveguide. P_{cl} and P_{wg} are all calculated in the post-processing step of HFSS simulation, directly from the 3-D electromagnetic field results.

Based on the simulated cold-circuit properties, Pierce linear theory is preliminarily employed to compute the small signal gain. Taking into account the phase velocity

dispersion, beam-wave interaction impedance, and cold-circuit attenuation, and applying a virtual electron beam condition, Pierce linear theory can be employed to calculate the small signal gain under simplified conditions [14, 15, 82].

2.2 Particle-in-cell simulation and optimization

From the cold-circuit analysis, a sets of structural parameters were obtained, which found the basis for us to further study the beam-wave interaction properties and optimize the performance of folded-waveguide slow-wave circuit with particle-in-cell (PIC) simulation. With PIC simulation, we can analyze slow-wave circuit in a more accurate and comprehensive way, for example the amplifier properties of the whole TWT can be verified under both linear and nonlinear conditions, and the simplification due to the absence of electron beam in the cold-circuit analysis can be overcome. PIC simulation is an effective method to model the folded waveguide slow-wave circuit, and the risk of design failure can be further reduced.

Within a slow-wave circuit circuit, the EM fields are determined by Maxwell's equations with the source current and charge densities, while the electrons are governed by the Newton's law or their relativistic version [15, 16, 42]. These equations are coupled together in the way that the EM fields are induced by the current and charges of the moving electrons, while the electrons move according to the EM fields [42]. To solve the governing self-consistent equations, simplified linear and nonlinear theories are applied under approximations, as to reduce the complexity of calculation [42]. In this way, the accuracy and credibility of the calculation will be undermined to a great extent. To provide better accuracy and credibility for analysis, PIC method is used to directly solve the self-consistent equations in meshed structure of the beam-wave interaction circuits [42].

In the PIC method, the arbitrary functions of charged particles are statically represented with discrete computer particles, and the computer particles exist in a continuum space and interact with EM fields through a discrete grid using interpolation [16, 42]. The brief PIC Scheme of the CST particle studio is shown in

fig.2.4 [83]. However, due to the complexity of solving the self-consistent equations inside the numerous meshed cells and tedious interpolations, the PIC method is more complicated and time-consuming than the linear and nonlinear theories. With the development of computing power of the modern computer and commercial simulator,

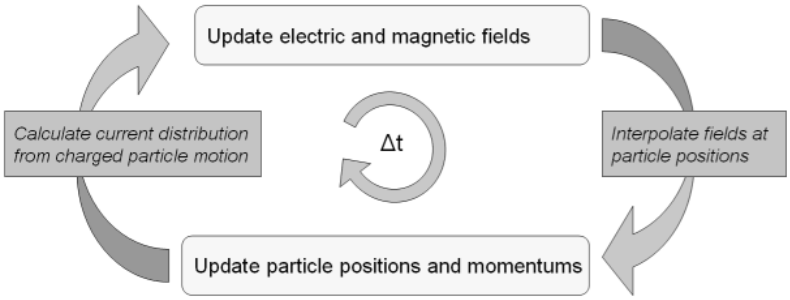

Figure 2.4 Brief scheme of the PIC simulation process

the PIC simulation for slow-wave circuits has been facilitated and is becoming more and more popular for the design of electron-tube devices.

In our analysis, the CST particle studio was employed to construct and simulate the 3-D folded-waveguide SWS model, and investigate the temporally and spatially continuous beam-wave interaction on the meshed structure, analyzing the frequency-dependent characteristics in the post-processing steps. Optimization with PIC method was also carried out. We applied the phase velocity taper near the output end of the circuit, to improve the output power and efficiency.

2.2.1 Constructing PIC model

The model of the folded-waveguide TWT is illustrated in Fig.2.5. An electron gun, input/output waveguide ports, a serpentine (folded) waveguide for slowing down the EM wave, a tunnel for the electron beam to pass through and a sever within the serpentine circuit for representing a concentrated attenuator are constructed in our PIC simulation model. The concentrated attenuator is employed to cut off the circuit between the input and output ports and significantly attenuates the EM wave in order

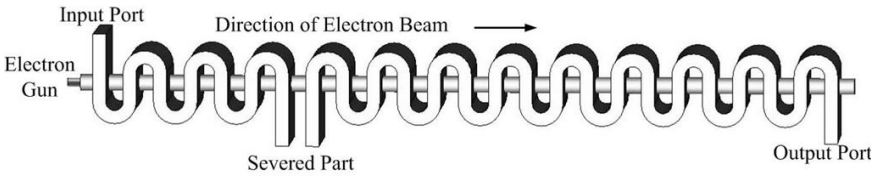

Figure 2.5 Particle studio model of folded waveguide slow-wave circuit. Two waveguide ports were built up on the "RF in" and "RF out", representing the input/output coupler.

to suppress backward wave oscillation. The concentrated attenuator is modeled in this way: the bending waveguide is removed at the sever position, and the two straight waveguides (dimension L_0, as shown in Fig.2.2 (a)) are lengthened outwards. The open boundary condition is applied onto the port of the straight waveguides so that both the forward and backward EM waves are perfectly absorbed. Thus, the concentrated attenuator model is an ideal one as there are no EM waves reflected from the open boundaries.

The PIC folded waveguide model consists of 64 periods of the serpentine

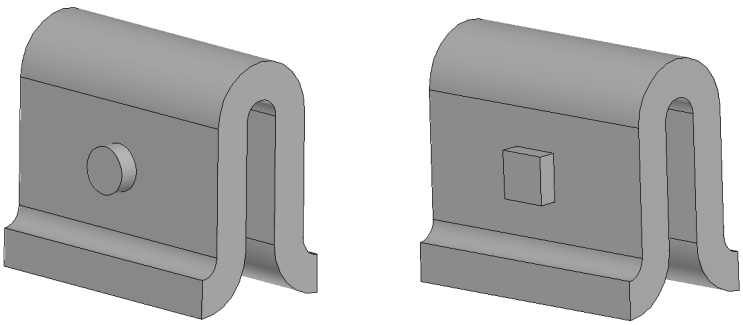

(a) (b)

Figure 2.6 Folded waveguide models with (a) circular cross-section and (b) square cross-section beam tunnel.

waveguide and has an axial length of 36 mm, and the severed part of the circuit locates at about one third of the total length from the input end. A simplified design of the focusing magnetic field is used in our PIC simulations, with a constant on-axis magnetic field of 1 T.

Two types of electron beam tunnel, with square or circular cross-section, are constructed on the folded waveguide model. Fig.2.6 shows two different models with different cross-section for the beam tunnel. A term “R/C” is defined to describe the ratio of the side length of square cross-section to the diameter of circular cross-section, as shown in fig.2.6, for beam tunnel. The models with square and circular cross-section of beam tunnel are named as R-tunnel model and C-tunnel model for short, respectively. The difference between these two types of beam tunnel with different cross-section is analyzed in the thesis as well. At first, a comparison between these two types of models was made within one pitch of circuit, based on the cold-circuit-simulation result. Then PIC simulation was employed to further analyze the amplifier performances of these two types of models.

In our PIC simulations, both single-frequency and multiple-frequency excitation signals were employed. To analyze the small-signal behavior, we apply a multiple-frequency excitation signal and obtain the response of discrete frequency points within the frequency band of interest through a single simulation, which reduces the simulation time considerably, efficiently predicting the 3-dB small-signal gain bandwidth. However, because of concern about high peak-to-average power in the multiple-frequency excitation signal, only single-frequency signals were applied to excite the circuit for the large-signal analysis.

2.2.2 PIC optimization with phase velocity taper

To extract even more kinetic energy from electron beam at the second half of folded waveguide circuit, after the electron beam has given some of its kinetic energy to the electromagnetic wave and is decelerated to some extent, the EM wave phase velocity need to be slowed down, in order to meet the synchronous condition required by ideal beam-wave interaction. Due to the unique structure of folded waveguide, it is very easy to merely lengthen the straight part of waveguide (L_0 in fig.2.2(a)) so as to elongate the EM wave path, without altering the characteristic impedance of the

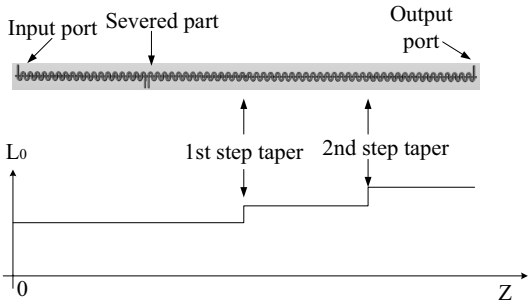

Figure 2.7 Sketch-map showing two-step reconfiguration of folded waveguide for EM wave phase velocity taper.

fundamental TE_{10} mode. This method of velocity taper eliminates any severe reflections of the forward wave due to impedance mismatches.

As illustrated in fig.2.7, the straight waveguide length L_0 is lengthened in a style of step transition, and the effective on-axis phase velocity of the EM wave is thereby decelerated. The electric field probe is also applied to monitor how the electric field grows with the length of the interaction circuit, for analyzing the electric field amplification along the circuit.

This page intentionally left blank

3 Development of SU-8 based Microfabrication Process for Folded Waveguide

SU-8 is a negative tone, epoxy-based photoresist, and it has been commonly used in micromachining microfluidics devices and Micro-Electro-Mechanical Systems (MEMS) devices, and as well as nanoprinting lithography technique, since developed by IBM at mid 1990s [41, 84-85]. Particularly, SU-8 photoresist is used to fabricate microstructure with high aspect ratio (HAR), as it is highly transparent in the ultraviolet (UV) region and nearly vertical sidewall can be achieved on SU-8 structures via UV lithography [41, 84-85]. Compared to another micromachining technique for HAR structures, i.e. X-ray LIGA, SU-8 based UV-LIGA has the advantage of low cost, fast process speed and better accessibility, since it does not require ultra expensive X-ray exposure machine and can be processed in almost every common clean room environment.

For its excellent micromachining capability, good optical properties and good mechanical & chemical stability, SU-8 photoresist has been applied to fabricate microwave and optical devices, such as filters, resonators and waveguides [6, 86-88]. Generally, the circuit loss for microwave waveguides depends greatly on the surface roughness of the sidewall of devices, which causes resistive loss inside waveguide. As we know, the skin depth of metal is in negative correlation to working frequency. When the skin depth of metal approaches the rms surface roughness, very severe resistive loss will occur on the metal waveguide due to the skin-effect [89]. Thus, this loss issue has produced a very demanding tolerance on the roughness control of machining process, when frequency reaches THz band.

In our experimental study for micromachining folded waveguide, two major goals were targeted, i.e. smooth sidewall of the waveguide and the circular cross-section beam tunnel.

3.1 Improvement of sidewall smoothness on SU-8 structure

During our experiments, an undesired surface morphology of sidewall, i.e. striated sidewall with striations vertical to the top surface (see fig.3.1), was encountered when the thick SU-8 structure was processed under the condition similar to that recommended by datasheet [90]. Therefore the sidewall surface roughness was

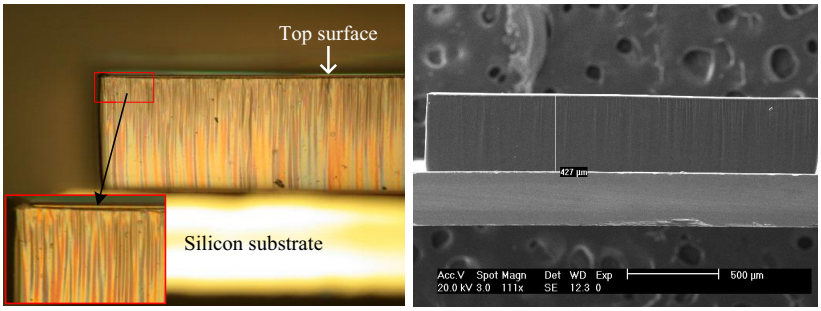

(a) (b)

Figure 3.1 (a) Optical and (b) SEM lateral view of SU-8 structure with striated sidewall morphology

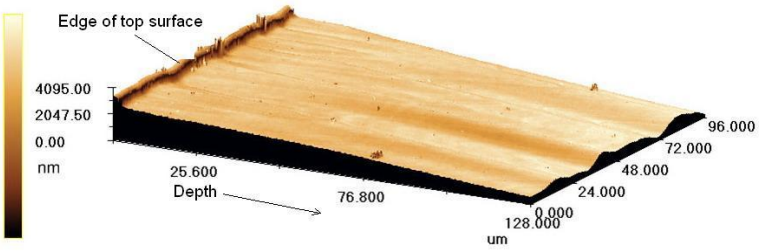

Figure 3.2 Three-dimension lateral view of striated sidewall right below the edge of top surface by CLSM

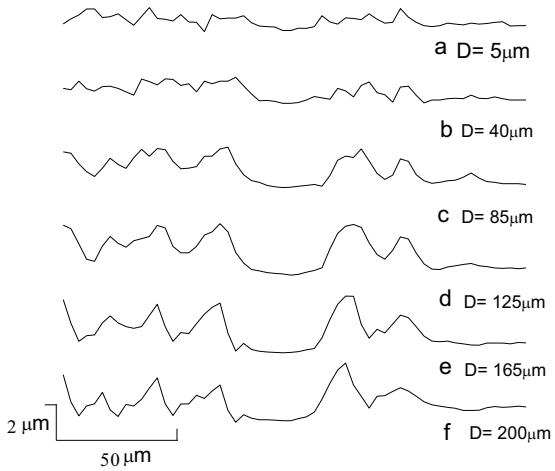

Figure 3.3 Depth-dependent edge profiles of cross-sectional surface and rms line roughness (R_q). D refers to the vertical distance from top surface to the measurement line, and the point-to-point sampling distance is 250nm. (a) R_q=0.309μm. (b) R_q=0.433μm. (c) R_q=0.712μm. (d) R_q=0.918μm. (e) R_q=0.873μm. (f) R_q=0.734μm.

dramatically increased, which will finally cause much severer resistive loss inside the waveguide. This experimental phenomenon appears on pictures of many literatures [91-95]. However, almost no morphology study has been made and the causes of these striations are still unknown.

Qualitative characterizations of striated sidewall were conducted by optical microscope and scanning electron microscope (SEM). Fig.3.1 (a) and (b) are obtained respectively by optical microscope and SEM for similar samples, illustrating that the sidewall is covered with severe striations. In fig.3.2, the magnified 3-D lateral view of sidewall right below the edge of top surface reveals a more explicit striated morphology of sidewall. Comparing to SEM pictures, the optical ones have higher contrast. Hence, they produce more prominent profile of sidewall striations.

Atomic force microscope (AFM) analysis is a popular 3-D measurement approach with very high resolution for surface morphology, but AFM can not conduct fast scanning on large area. And furthermore, the limitation of vertical measurement (maximum 1μm) of the AFM we used is below the maximum peak-to-valley roughness Rp-p (up to 3.6μm) on striated sidewall. That is the reason why we

employed confocal laser scanning microscope (CLSM), instead of AFM, to analyze the 3-D morphology of striated sidewall. CLSM has faster scanning speed and larger vertical measurement range, but lower vertical resolution (10nm) and transverse resolution (120nm) than ordinary AFM.

Based on the scanned data from CLSM, depth-dependent edge profiles of cross-sectional surface and rms line roughness were analyzed. The rms line roughness Rq is defined as below:

$$R_q = \sqrt{\frac{1}{N}\sum_{N}(Z_n - Z_{ave})^2} \tag{3-1}$$

where N represents the amount of measured points, Z_n and Z_{ave} are the height of the nth point and average height of N points, respectively.

Quantitative characterization was carried out on the striated sidewall by CLSM, and the depth-dependent sidewall line roughness for the striated sample is shown in fig.3.3. We applied CLSM to analyze both the 3-D sidewall morphology and depth-dependent line roughness along the sidewall. Based on the morphology analysis, the possible causes of sidewall striations were discussed. Counter measures were also employed to reduce the striated effect of sidewall. Through increasing the post-exposure bake (PEB) conditions, i.e. raising the temperature and prolonging the baking time, the striated sidewall surface is flatten. Thus the sidewall smoothness is improved to a great extent.

3.2 Novel process development for micromachining folded waveguide

Another critical issue for our ultra-thick SU-8 based micromachining process development is how to machine the hollow beam tunnel for the folded waveguide circuit. As we know, the electron beam tunnel has very different dimensions from that of the serpentine (folded) waveguide. In addition, the beam hole existing on the center of the broad wall of the straight part of the waveguide greatly complicates the

microfabrication process for the folded waveguide, since additional processing steps are required and more alignment error could be introduced..

3.2.1 Normal process for fabricating beam tunnel for folded-waveguide circuit

In order to fabricate the hollow beam tunnel together with the serpentine waveguide, several methods were proposed and employed to machine it [19, 20, 32]. The existing processes for machining hollow beam tunnel fall into two types. One type of processes is using photolithography technique to form the mold of the beam tunnel, while another type is to machine the beam tunnel via a different technique rather than photolithography, like micro-EDM (Electrical Discharging Machining) after fabricating the serpentine waveguide.

The first type of processes has an advantage since photolithography is a widely-used precise pattern transfer technique. However, the unique structure of folded waveguide cannot be formed in a single photolithography step. Instead, the folded waveguide is divided into two symmetric halves, and fabricated separately. For each half, the half beam tunnel and the half serpentine waveguide are patterned on different step with photolithography, respectively, as they have very different thickness from the perspective of microfabrication. The symmetric halves of folded waveguide are aligned together after each half finished. One of the disadvantages of this process is that additional alignment errors and machining complexity are involved. Typical examples of this process are based on two-step LIGA and DIRE [13, 20, 32]. Another apparent disadvantage is that only a beam tunnel with rectangular or square cross-section can be obtained, because photolithography is a two-dimensional pattern transfer technique.

Another type of process is to fabricate the serpentine waveguide with photolithography and electroplating at first, and then to create the hollow beam tunnel with a different technique, for example micro-EDM. The advantage is that fever photolithographic steps are involved, which will simplify the process to a certain extent. Micro-EDM sounds a plausible method for micromachining long and narrow

tunnel. But as mentioned in reference, the bur-clogging problem inside serpentine waveguide occurred during micro-EDM process, severely distorts the LIGA-fabricated folded-waveguide structure, therefore prevent the application of micro-EDM for machining long tunnel with circular cross-section [20].

3.2.2 Novel process for micromachining circular cross-section beam tunnel

To fabricate the long and narrow centimeters-long beam tunnel of the circular cross-section, we applied optical fiber embedment as the sacrificial structure for the beam tunnel in the ultra-thick SU-8 process. The brief process flow is designed as listed in fig.3.4. At least two times spin-coating of SU-8 photoresist and multiple photolithography are required in this process. The optical fiber is embedded between two steps of spin-coating. The serpentine waveguide mold is obtained at a single photolithographic step. A comparison between the novel process we proposed and the normal SU-8 based UV-LIGA process is illustrated in fig.3.5. In the normal fabrication procedure, folded waveguide is divided into two symmetric halves, and fabricated individually. For each half, the mold of beam tunnel (with rectangular cross-section) and the mold of serpentine waveguide should be formed separately through two-step coating and lithography, as given in the upper picture of fig.3.5(a). After electroplating of copper, the mold will be removed, and the two symmetric halves need to be aligned together (see the lower two pictures of fig.3.5(a)). While for our novel fabrication procedure, a sacrificial structure of beam tunnel—the optical fiber is embedded in the SU-8 mold of serpentine waveguide, as shown in the upper picture of fig.3.5(b). After development of photoresist, electroplating of copper will

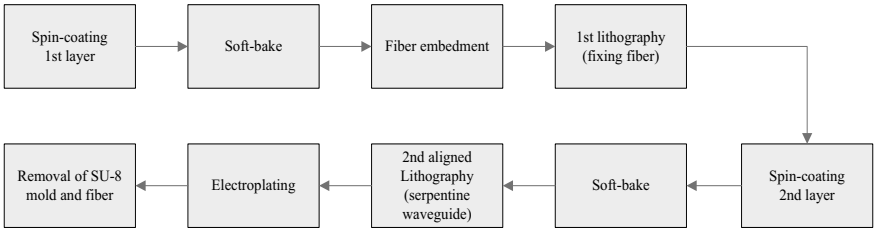

Figure 3.4 Schematic flow chart for fabricating folded waveguide with circular cross-section beam tunnel.

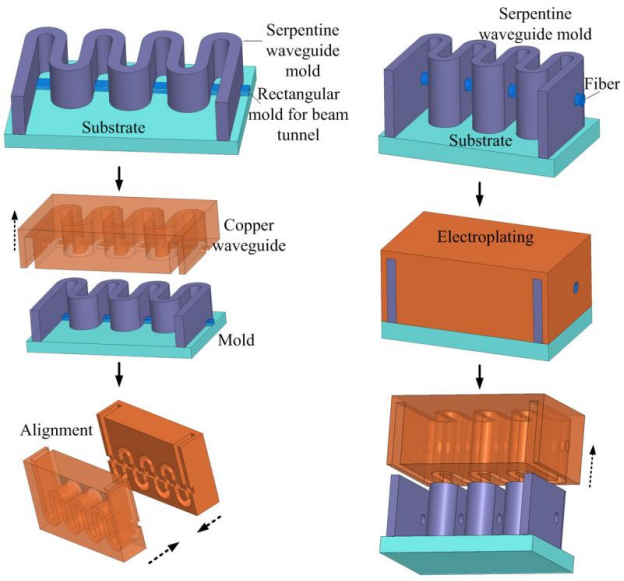

(a) (b)

Figure 3.5 Schematic chart of (a) normal procedure and (b) novel procedure for fabricating copper folded waveguide.

take place. The fiber need to be dissolved in hydrofluoric acid following electroplating, and then the SU-8 mold need to be removed, as revealed in the lower two pictures of fig.3.5(b).

Because the fiber is very thin and flexible, it is difficult to fix the fiber in position due to strong stress introduced in the SU-8 photoresist during baking. In order to fix the fiber in position, we designed additional process steps and introduced additional structures to keep the fiber in position. As illustrated in fig.3.6, we introduced pillar-pairs before the embedment step of the fiber, and these small pillar-pairs and the following exposure step will keep the fiber against the in-plane deflection.

The thickness uniformity of SU-8 layer is another important factor for the ultimate full-copper folded waveguide and for the out-of-plane bending of the embedded fiber, because it determines the structural uniformity across the whole circuit. We applied additional processing steps to improve the thickness uniformity for the ultra-thick SU-8 structure.

For the ordinary spin-coating process, the thickness of photoresist and uniformity

of thickness seems to be contradictory, as the thickness achieved is proportional to the viscosity and inversely proportional to the spin-speed. Therefore, to achieve ultra-thick SU-8 structure, both high-viscosity photoresist and low spinning speed are required in the spin-coating process. For example, to obtain a layer of ~500 micrometer, usually we have to use very viscous SU-8 photoresist Microchem model 2150 and spin-speed as low as 1000 rpm [90]. The side effect of high viscosity and low spinning speed is obvious: The control of thickness uniformity becomes more difficult. Severe edge bead will be created near the edge of the wafer right after spin-coating, and this will result in poor contact for the contact lithography and severe out-of-plane bending of the fiber embedded in the SU-8 photoresist. The thickness difference is estimated to be > 80μm across the SU-8 coated on a 4-inch silicon wafer, then the average thickness is around 500μm.

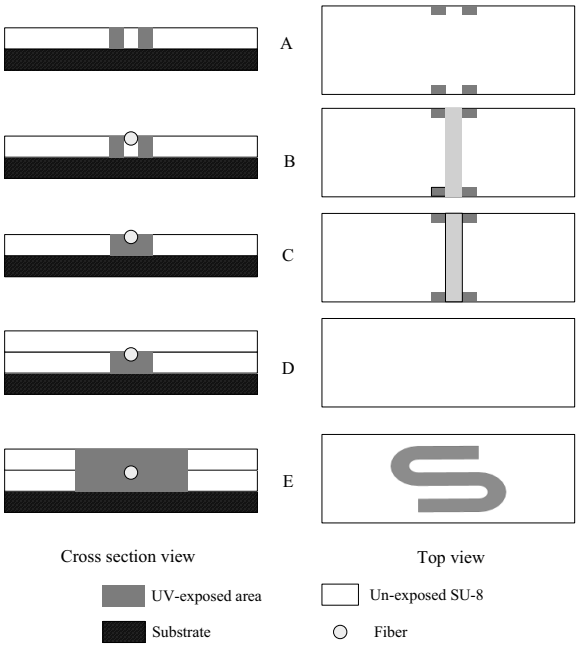

Figure 3.6 Fiber embedment and pattern transfer procedure: A. forming of micro pillars by UV-exposure for fixing fiber in 1st SU-8 layer; B. placement of fiber; C. UV-exposure for fixing fiber in position; D. coating of 2nd SU-8 layer; E. pattern transfer of serpentine structure onto ultra-thick SU-8 layer

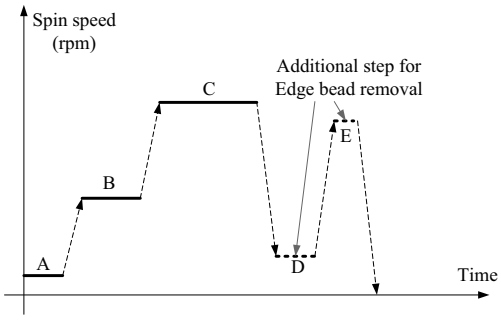

Figure 3.7 Spin-speed profile versus time. *A* is the initial spinning step; followed by step *B* to further spread the photoresist at a higher speed; then reach the highest spin-speed and stay for ~30 second. During additional step *D*, acetone is sprayed on the edge of SU-8 layer and dissolves it; then accelerated to a high speed again to spin off the acetone together with the edge bead of the layer.

To minimize the impact of edge bead, we applied two additional steps to remove the edge bead following the ordinary spin-coating, as illustrated in fig.3.7. During step *D*, we use syringe filled with acetone and spray the acetone onto the edge of SU-8 layer through a needle, when the substrate is kept on a very low spinning speed. The acetone will dissolve the SU-8 and reduce the viscosity. Then a higher speed spinning step is applied for ~10 seconds, to spin off the low-viscosity part of the SU-8 layer dissolved by acetone, resulting in a layer without edge bead. As a consequence, the thickness uniformity of the SU-8 structure can be improved greatly, and the out-of-plane bending of the fiber embedded inside SU-8 structure can be relieved.

This page intentionally left blank

4 Summaries and Outlooks

Summaries of the articles

In our research, both theoretical analysis and electromagnetic field simulations have been carried out on the folded-waveguide slow-wave circuit for the Terahertz traveling-wave tubes. Ultra-thick SU-8 process is employed to fabricate the folded waveguide mold, and the process development also helps to improve the smoothness of sidewall for the SU-8 folded waveguide mold. To fabricate the longitudinal electron beam tunnel across the whole folded waveguide, we applied optical fiber embedment in the SU-8 photoresist. Through our study, better knowledge is accumulated on the design of folded waveguide circuit， simulation and optimization for both the cold circuit properties and beam-interaction circuit properties of this slow-wave circuit, which can be used as a basis for developing Terahertz folded-waveguide traveling-wave tubes. Our research efforts and new ideas on the microfabrication process development for miniaturized folded waveguide circuit contribute to the development of folded waveguide circuits. The summaries of four articles and the major conclusion of the thesis are given as follow.

1 Parametric Simulation and Optimization of Cold-test Properties for a 220GHz Broadband Folded Waveguide Traveling-wave Tube

The cold-circuit analysis and parametric simulation were described in the first paper. The analysis on cold circuit properties of folded waveguide circuit reveals a very broad pass-band of ~80GHz, which refers to the band between the cut-off frequency and the 1st stop-band. How the structural parameters of folded waveguide circuit influence the cold-circuit (without presence of electron beam) properties is also studied and well understood via parametric analysis based on the electromagnetic field simulations. Optimization of the key cold-circuit property, i.e. the beam-wave

interaction impedance, was carried out on some crucial structural parameters with discrete matrix method, to achieve a balance between the requirements for high gain and broadband. Optimized cold-circuit properties also pave the way for further beam-interaction circuit simulation and optimization. Pierce small signal theory was also used to predict the linear gain and three-dB bandwidth based on the simulated cold circuit properties.

2 Particle-in-cell Simulation and Optimization for a 220GHz Folded-Waveguide Traveling-wave Tube

In the second paper, the beam-wave interaction simulation and optimization for a 220GHz central frequency folded-waveguide circuit were presented. Beam-interaction circuit simulation (with real electron beam present), i.e. particle-in-cell (PIC) simulation were made based on the optimized parameters from the cold-circuit simulations and optimizations. Not only the amplifier properties of the folded waveguide traveling wave tube were verified by PIC simulation, but also further optimizations on the output power and gain of traveling-wave tube were able to carry out with the help of PIC simulation. Phase velocity taper of electromagnetic wave near the output end is proven as an effective way to improve the gain, output power and efficiency. The optimized peak saturate output power under loss-free simulation, is ~70W at the central frequency. Our optimized results show that up to 70% improvement of the saturated output power can be achieved via proper phase velocity taper. As predicted by the loss-free PIC simulation, our optimized design has a 3-dB bandwidth of ~15 GHz and saturated output peak power of 70W for continuous wave.

The impact of the transverse shape of electron beam tunnels, i.e. square and circular cross-section, on the amplifier characteristics of folded waveguide traveling-wave tube was also studied. Our PIC analysis reveals that the folded-waveguide circuit with circular-cross-section tunnel provides better beam-wave interaction than the one with square-cross-section tunnel, given the same beam fill factor. With circular-cross-section beam tunnel, folded waveguide circuit exhibits higher gain and

efficiency, and similar bandwidth in our PIC simulation, comparing to the one with square-cross-section. This result implies that using circular cross-section tunnel is possibly a good choice to enhance beam-wave interaction within folded-waveguide slow-wave circuit.

3 Characterizing and smoothing of striated sidewall morphology on UV-exposed thick SU-8 structures for micromachining millimeter wave circuits

In the third published paper, the analysis on striated sidewall profile and the effort on smoothing the sidewall of the ultra-thick SU-8 structure were reported. We quantitatively analyzed the sidewall striated morphology via CLSM and found out the probable root cause for the sidewall striation. The sidewall smoothness is greatly improved through proper control of the post-exposure-bake condition, i.e. the baking temperature and time. The RMS line sidewall roughness is decreased from ~1 μm to ~70 nm. We also carried out analysis on the striated sidewall profile of the SU-8 mold via conformal laser scanning microscopy. It is reasonable to believe that dynamic roughening process during development contribute a lot to the striation of sidewall profile. With the help of atomic force microscope, we found out that the sample fabricated with optimized process parameters has RMS sidewall surface roughness as low as 2.6 nm, which ensures better controlling the conduction loss of the resulting full-copper folded waveguide circuit.

4 A Novel Approach to Micromachine Terahertz Folded-Waveguide Slow-wave Structure with Beam Tunnel of Circular Cross- section

In the last manuscript, the development of a novel microfabrication process for machining folded waveguide with circular cross-section was presented. Considering its benefit, we aim at developing a new process for machining circular-cross-section beam tunnel for the folded-waveguide circuit. A novel process was proposed in our study. Optical fiber was embedded onto the SU-layer as sacrificial structure for the cylindrical hollow beam tunnel. We achieved well-confined fiber embedment inside

our SU-8 mold. The thickness uniformity of SU-8 structure is also improved. This novel process also guarantees lower alignment error during micromachining.

Outlooks

As the PIC simulation tool we used does not support lossy circuit simulation well, further study of folded waveguide circuit needs more comprehensive simulation on the lossy circuit, to better verify the design of folded waveguide traveling-wave tube amplifier.

Further process developments are also required, including the low-stress electroplating of copper on the ultra-thick SU-8 structure, the removal of optical fiber after electroplating and the fly-cutting to obtain the desired thickness for the copper structure.

High frequency measurement is also needed after fabrication of the entire folded waveguide. The reasonable way is to measure the eigenfrequency of the folded waveguide for verifying the cold circuit properties with the simulated results before the TWT device can be finished.

References

[1] P. H. Siegel, "Terahertz technology", *IEEE Trans. on Microwave Theory and Techniques*, vol.50 no.3, pp.910-928, 2002.

[2] D. Dragoman and M. Dragoman, "Terahertz fields and applications", *Progress in Quantum Electronics*, vol.28 issue 1, pp.1-66, 2004

[3] M. Tonouchi, "Cutting-edge terahertz technology", *Nature Photonics*, 1, 97 - 105 (2007)

[4] B. Ferguson and X. C. Zhang, "Materials for terahertz science and technology", *Nature Materials* 1, 26 - 33 (2002).

[5] B. S. Williams, "Terahertz quantum-cascade lasers", *Nature Photonics* 1, 517 - 525 (2007)

[6] R. L. Ives, "Microfabrication of high-frequency vacuum electron devices", *IEEE Transactions on plasma science*, Vol.32 No. 3, Part 1, pp.1277-1291, Jun. 2004

[7] J. Hebling, K.L. Yeh and M. C. Hoffmann et al., "High-Power THz Generation, THz Nonlinear Optics, and THz Nonlinear Spectroscopy", *IEEE Journal of Selected Topics in Quantum Electronics*, Vol.14 No.2, pp.345-353, 2008

[8] S. L. Dexheimer, "Terahertz Spectroscopy-principles and applications", CRC press, 2007

[9] K. Miyamoto, S. Ohno, and M. Fujiwara et al. , "Optimized terahertz-wave generation using BNA-DFG," Opt. Express 17, 14832-14838 (2009)

[10] V. L. Granatstein, R. K. Parker, and C. M. Armstrong, "Vacuum electronics at the dawn of the twenty-first century", *The Proceedings of the IEEE*, Vol.87 No.5, pp.702-716, May 1999

[11] R. K. Parker, R. H. Abrams, and B. G. Danly et al., "Vacuum electronics", *IEEE Transactions on Microwave Theory and Techniques*, Vol.50 No.3, pp.835-845, Mar. 2002

[12] V. M. Lubecke, K. Mizuno and G. M. Rebeiz, "Micromachining for terahertz applications", *IEEE Transactions on Microwave Theory and Techniques*, Vol.46 No.11, pp.1821-1831, Nov. 1998

[13] www.teraphysics.com

[14] A. G. Glimour, Jr., "Principles of traveling wave tubes", *Artech House*, 1994

[15] S. E. Tsimring, "Electron beams and microwave vacuum electronics", *Wiley-Interscience*, 2007

[16] B. N. Basu, "Electromagnetic theory and applications in beam-wave electronics", *World Scientific*, 1995

[17] C.L. Kory, J.H. Booske, J.H., and W. Lee et al., "THz radiation using high power, microfabricated, wideband TWTs", *Microwave Symposium Digest, 2002 IEEE MTT-S International*, Vol.2, pp. 1265-1268, Aug. 2002

[18] S. Bhattacharjee, J.H. Booske, and C.L. Kory et al. "THz radiation using compact folded waveguide TWT oscillators", *Microwave Symposium Digest, 2003 IEEE MTT-S International*, Vol.2, pp.1331-1334, Jun.2003

[19] S. Bhattacharjee, J. H. Booske, and C. L. Kory et al., "Folded Waveguide Traveling-wave Tube Sources for Terahertz Radiation", *IEEE Transactions on Plasma Science*, vol. 32, issue 3, part 1, pp.1002-1014, June 2004

[20] J. Tucek, M. Basten, and D. Gallagher et al., "220 GHz Folded Waveguide Circuits for High Power Amplifiers", *Proceedings of 10th IEEE International Vacuum Electronics Conference*, pp.108-109, Rome, April 2009

[21] Y. Shin, L. Barnett, and N. Luhmann Jr., "Experimental, Numerical and Analytical Studies of the Staggered Double Vane Structure for THz Application", *Proceedings of 10th IEEE International Vacuum Electronics Conference*, pp.106-107, Rome, April 2009

[22] Y. Shin, L. Barnett, and D. Gamzina et al., "Terahertz vacuum electronic circuits fabricated by UV lithographic molding and deep reactive ion etching", *Appl. Phys. Lett*. 95, 181505 (2009)

[23] A. Di Carlo, C. Paoloni, and F. Brunetti et al., "The European Project OPTHER for the Development of a THz Tube Amplifier (Keynote Presenation)", *Proceedings of 10th IEEE International Vacuum Electronics Conference*, pp.100-101, April 2009

[24] J.A. Dayton Jr., C.L. Kory, and G.T. Mearini et al., "A 650 GHz helical BWO", *Vacuum Electronics Conference, 2008. IVEC 2008. IEEE International*, pp.396-397, Apr.2008

[25] J.T. Mendel, "Helix and coupled-cavity traveling-wave tubes", *Proceedings of the IEEE*, vol.61 no.3, pp.280- 298, 1973

[26] A.F. Harvey, "Periodic and Guiding Structures at Microwave Frequencies", Microwave Theory and Techniques, IRE Transactions on, vol.8 no.1, pp.30-61, 1960

[27] S. Lucyszyn, "Accurate CAD modelling of metal conduction losses at terahertz frequencies", *Electron Devices for Microwave and Optoelectronic Applications, 2003. EDMO 2003. The 11th IEEE International Symposium on* , pp.180- 185, Nov. 2003

[28] J.A. Dayton Jr., C.L. Kory, and G.T. Mearini et al., "Applying microfabrication to helical vacuum electron devices for THz applications", *Vacuum Electronics Conference, 2009. IVEC '09. IEEE International*, pp.41-44, Apr.2009

[29] A. S. Srivastava, J. K. Sattorov, M. A. Kwon, "100GHz LIGA-fabricated coupled-cavity device", *Proceedings of 10th IEEE International Vacuum Electronics Conference*, pp.102-103, April 2009

[30] G. Doher, D. Gagne, and D. Gallagher, "Serpentine waveguide TWT", *International Electron Devices Meeting, Technical Digest*, pp.485-488, 1987

[31] M.J. Madou, "Foundamentals of Microfabrication 2nd edition", CRC-Press, 2005

[32] Y.M. Shin, J.K. So and S.T. Han et al., "Microfabrication of millimeter wave vacuum electron devices by two-step deep-etch x-ray lithography", *Appl. Phys. Lett.* **88**, 091916 (2006)

[33] C. Mack, "Fundamental Principles of Optical Lithography: The Science of Microfabrication", Wiley, 2007

[34] J.H. Booske, M.C. Converse, and C.L. Kory et al., "Accurate parametric modeling of folded waveguide circuits for millimeter-wave traveling wave tubes," *Electron Devices, IEEE Transactions on,* vol.52 no.5, pp.685- 694, 2005

[35] A.K. Sharma, R.K. Sharma, and G. Dixit et al., "Design of RF structure for a terahertz source", *Recent Advances in Microwave Theory and Applications, 2008. MICROWAVE 2008. International Conference on*, pp.185-187,Nov. 2008

[36] R. Zheng and X. Chen, "Parametric Simulation and Optimization of Cold-test Properties for a 220 GHz Broadband Folded Waveguide Traveling-wave Tube", *Journal of Infrared, Millimeter and Terahertz Waves,* Vol.30, No.9, Sep. 2009 pp.945-958

[37] F. Malek, "Design and analytical modeling of folded waveguide traveling wave tube", *Nuclear Instruments and Methods in Physics Research A* 612 (2009) 176–186

[38] Z. Chen, Y. Cheng, and Y. Wang et al., "Fast design and cold-circuit properties simulation for the slow wave structure of a 0.14 THz broadband folded waveguide traveling wave tube", *Journal of Infrared Millimeter and Terahertz Waves*, Vol.31 no.8, pp.926-933, 2010

[39] S.T. Han, J.I. Kim, and G.S. Park, "Design of a folded waveguide traveling-wave tube", MICROWAVE AND OPTICAL TECHNOLOGY LETTERS, Vol.38 no.2, pp.161-165, 2003

[40] B. Qu, and J. Feng, "Design and Simulation of 140GHz Folded Waveguide TWT Slow-wave Structure," Infrared Millimeter Waves and 14th International Conference on Teraherz Electronics, 2006. IRMMW-THz 2006. Joint 31st International Conference on, pp.226-226, Sep.2006

[41] M. Despont, H. Lorenz, and N. Fahrni et al., "High-aspect-ratio, ultrathick, negative-tone near-uv photoresist for MEMS applications," Micro Electro Mechanical Systems, 1997. MEMS '97, Proceedings, IEEE., Tenth Annual International Workshop on, pp.518-522, Jan. 1997

[42] T.M. Antonsen, A.A. Mondelli, and B. Levush et al., "Advances in modeling and simulation of vacuum electronic devices", *Proceedings of the IEEE*, Vol.87 No.5, pp.804-839, 1999

[43] C.L. Kory, and J.A. Dayton Jr. ,"Accurate cold-test model of helical TWT slow-wave circuits," *Electron Devices, IEEE Transactions on,* vol.45 no.4, pp.966-971, 1998

[44] H.J. Ha, S.S. Jung, and G.S. Park, "Theoretical study for folded waveguide traveling wave tube", *International journal of Infrared and Millimeter Waves,* Vol.19 no.9, pp.1229-1245, 1998

[45] H. Lorenzyz , M. Despontxk, and N. Fahrniy et al., "SU-8: a low-cost negative resist for MEMS", *Journal of Micromechanics and Microengineering,* Vol.7, No.3, pp.121-124, 1997

[46] J.Ruano-Lopez , M. Aguirregabiria, and M. Tijero et al., "A new SU-8 process to integrate buried waveguides and sealed microchannels for a Lab-on-a-Chip", *Sensors and Actuators B: Chemical*, Vol. 114, Issue 1, pp.542-551, 2006

[47] P. Pengvanich, D. Chernin, and Y. Lau et al., "Effect of Random Circuit Fabrication Errors on Small-Signal Gain and Phase in Traveling-Wave Tubes", *IEEE TRANSACTIONS ON ELECTRON DEVICES*, VOL. 55, NO. 3, pp.916-924, 2008

[48] S. Lucyszyn, "Investigation of anomalous room temperature conduction losses in normal metals at terahertz frequencies", *IEE Proceedings on Microwaves, Antennas and Propagation*, Vol.151 Issue.4, 321-329, 2004

[49] W. Wang, Y. Wei, and G. Yu et al., "Review of the Novel Slow-Wave Structures for High-Power Traveling-Wave Tube", *International Journal of Infrared and Millimeter Waves*, Vol.24, No.9, pp.1469-1484, 2003

[50] J. Feng, J. Cai, and X. Wu, "Design investigation of 10W W-band folded waveguide TWT", *Vacuum Electronics Conference, 2007. IVEC '07. IEEE International ,* pp.1-2, 2007

[51] A. Theiss, C. Meadows, and R. True, "Experimental Investigation of a Novel Circuit for Millimeter-Wave TWTs", *IEEE TRANSACTIONS ON ELECTRON DEVICES,* VOL.54, NO.5, pp.1054-1060, 2007

[52] J. He, Y. Wei, and Z. Lu,"Investigation of a Ridge-Loaded Folded-Waveguide Slow-Wave System for the Millimeter-Wave Traveling-Wave Tube", *IEEE TRANSACTIONS ON PLASMA SCIENCE*, Vol.38, No.7, pp.1556-1562, 2010

[53] F. Malek, "THE ANALYTICAL DESIGN OF A FOLDED WAVEGUIDE TRAVELING WAVE TUBE AND SMALL SIGNAL GAIN ANALYSIS USING MADEY'S THEOREM", *Progress In Electromagnetics Research*, PIER 98, pp.137-162, 2009

[54] V. Heinen, K. Kreischer, and M. Basten et al., "Vacuum Electronics Development at Northrop Grumman", *Vacuum Electronics, 2003 4th IEEE International Conference on*, pp.319, 2003

[55] J. Tucek, M. Basten, and D. Gallagher et al., "Sub-millimeter and THz power amplifier development at northrop grumman", *Vacuum Electronics Conference (IVEC), 2010 IEEE International,* pp.19-20, 2010

[56] O. Makarova1, R. Divan, and J. Tucek, "Fabrication of Solid Copper 220 GHz Folded Waveguide Circuits by UV Lithography", *Vacuum Electronics Conference (IVEC), 2010 IEEE International*, pp.183-184, 2010

[57] J. He, Y. Wei , and Y. Gong et al., "Linear Analysis of Folded Double-Ridged Waveguide Slow-Wave Structure for Millimeter Wave Traveling Wave Tube", *CHIN. PHYS. LETT.* Vol. 26, No. 11 (2009) 114103, 2009

[58] M. Sumathy, K. J. Vinoy, and S. K. Datta, "Analysis of Ridge-Loaded Folded-Waveguide Slow-Wave Structures for Broadband Traveling-Wave Tubes", *IEEE TRANSACTIONS ON ELECTRON DEVICES*, VOL. 57, NO. 6, pp.1440-1446, 2010

[59] C. Zhang, Y. Gong, and H. Gong et al., "Investigation of the Dielectric-Loaded Folded Waveguide Traveling-Wave Tube Amplifier", *Journal of Infrared, Millimeter and Terahertz Waves,*Vol.30, No.10, pp.1027-1037, 2009

[60] M. Liao, Y. Wei, and J. He, "Analysis of a Novel Ka-band Folded Waveguide Amplifier for Traveling-Wave Tubes", *CHIN. PHYS. LETT.* Vol. 26, No. 11 (2009) 114207, 2009

[61] M. Liao, Y. Wei, and Y. Gong et al., "A Rectangular Groove-Loaded Folded Waveguide for Millimeter-Wave Traveling-Wave Tubes", *IEEE TRANSACTIONS ON PLASMA SCIENCE*, Vol.38, No.7, pp.1574-1578, 2010

[62] J. He, Y. Wei, and Y. Gongt al., "Investigation of a W band novel folded-waveguide TWT", Vacuum Electron Sources Conference and Nanocarbon (IVESC), 2010 8th International, pp.96-97, 2010

[63] A. Xu, W. Wang and Y. Wei et al., "The study of synchronization in the periodic nonuniform folded waveguide", *Chinese Physics B*, Vol.18 No.2, pp.810-814, 2009

[64] J. He, Y. Wei, and Y. Gong et al., "Analysis of a 140GHz Two-Section Folded Waveguide Traveling-Wave Tube", *Photonics and Optoelectronic (SOPO), 2010 Symposium on*, pp.1-4

[65] A. Theiss, C. Meadows, and R. Freeman et al., "High-Average-Power W-band TWT Development", *IEEE TRANSACTIONS ON PLASMA SCIENCE*, Vol.38, No.6, pp.1239-1243, 2010

[66] H. Gong, Y. Gong, and T. Tang et al., "20.3: High Power Ka-band Folded Waveguide Traveling-Wave Tube", *Vacuum Electronics Conference (IVEC), 2010 IEEE International*, pp.499-500, 2010

[67] G. Vela, M. Miller, and R. Grow, "9.1: Terahertz Backward-Wave Oscillator Slow-Wave Circuits ", *Vacuum Electronics Conference (IVEC), 2010 IEEE International*, pp.179-180, 2010

[68] R. Stuart, A. Al-Shamma'a, and C. Wright, "Compact tuneable microwave terahertz source", *High Power RF Technologies, 2009. IET. Conference on*, pp.1-4, 2009

[69] A. Aksenchyk, A. Kurayev, and I. Kirinovich, "P4-8: Folded Waveguide TWT Frequency Characteristics in the Range 600-3000 GHZ", *Vacuum Electronics Conference (IVEC), 2010 IEEE International*, pp.461-462, 2010

[70] J. Tucek, D. Gallagher, and K. Kreischer et al., "A compact, high power, 0.65 THz source", *Vacuum Electronics Conference, 2008. IVEC 2008. IEEE International*, pp.16-17, 2008

[71] M. Mineo and C. Paoloni, "Corrugated Rectangular Waveguide Tunable Backward Wave Oscillator for Terahertz Applications", *IEEE TRANSACTIONS ON ELECTRON DEVICES*, Vol.57, No.6, pp.1481-1481, 2010

[72] M. Mineo and C. Paoloni, "Double-Corrugated Rectangular Waveguide Slow-Wave Structure for Terahertz Vacuum Devices", *IEEE TRANSACTIONS ON ELECTRON DEVICES*, Vol.57, No.11, pp.3169-3175, 2010

[73] Y. Shin, L. R. Barnett, and N. C. Luhmann Jr., "Strongly confined plasmonic wave propagation through an ultrawideband staggered double grating waveguide", *Appl. Phy. Lett.* 93, 221504 (2008)

[74] Y. Shin, L. Barnett, and N. Luhmann et al., "Phase-shifted travelingwave-tube circuit for ultrawideband high-power submillimeter-wave generation", *IEEE TRANSACTIONS ON ELECTRON DEVICES*, Vol.56, No.5, pp.706-712, 2009

[75] R. Zheng, and X. Chen, "Design and 3-D simulation of microfabricated folded waveguide for a 220GHz broadband traveling-wave tube application", *Vacuum Electronics Conference, 2009. IVEC '09. IEEE International*, pp.135-136, 2009

[76] Y. Li, P. Kirby, and J. Papapolymerou, "Silicon Micromachined W-Band Folded and Straight Waveguides Using DRIE Technique", *Microwave Symposium Digest, 2006. IEEE MTT-S International* , pp.1915-1918, 2006

[77] C. Lee, K. Jiang, andG. Davies, "Sidewall roughness characterization and comparison between silicon and SU-8 microcomponents", *Materials Characterization* 58 (2007) 603–609

[78] K. Vora1, B. Lochel, and E. Harvey et al., "AFM-measured surface roughness of SU-8 structures produced by deep x-ray lithography", *J. Micromech. Microeng.* 16 (2006) 1975–1983

[79] N.Marcuvitz, "Waveguide Handbook", Peter Peregrinus Ltd, 1986,pp.333-334,364-365

[80] D. M. Pozar, "Microwave engineering (second edition)" ,Wiley, 1998, pp.94-95

[81] S. Liu, "Study of propagation characteristics for folded waveguide TWT in millimeter wave", I*nternational Journal of Infrared and Millimeter Waves* 21(4), 655–660 (2000).

[82] S. G. Liu, H. F. li, W. X. Wang and Y. L. Mo, "Introduction to microwave electronics", National defense industry press, 1985 (in Chinese).

[83] CST Particle Studio Online Help, version 2009

[84] A. del Campo and C. Greiner, "SU-8: a photoresist for high-aspect-ratio and 3D submicron lithography", *Journal of Micromechanics and Microengineering*, Vol.17 Issue 6, June 2007, R81-R95.

[85] SU-8: Thick photo-resist for MEMS, http://memscyclopedia.org/su8.html

[86] K. Jiang, M.J. Lancaster, I. Llamas-Garro and P. Jin, "SU-8 Ka-band filter and its microfabrication", *Journal of Micromechanics and Microengineering*, Vol.15, No.8, August 2005, pp.1522-1526.

[87] A. Ismail and R.S.A Raja Abdullah, "Micromachined W-band rectangular waveguide utilising SU-8", *International Journal of Engineering and Technology*, Vol. 4, No.2, 2007, pp.245-252

[88] T. C. Sum, A. A. Bettiol, J. A. van Kan, F. Watt E. Y. B. Pun and K. K. Tung, "Proton beam writing of low-loss polymer optical waveguides", *APPLIED PHYSICS LETTERS*,Vol.83, No.9, September 2003, pp.1707-1709

[89] R. Brown, "RF/microwave hybrids: basics, materials and processes", Klumer Academic Publishers, 2004, pp.49-52

[90] SU-8 datasheet, http://www.microchem. com/products/pdf/SU-82000DataSheet2100and2150Ver5.pdf

[91] R. Ruhmann, G. Ahrens, and A. Schuetz et al., "Reduction of internal stress in a SU-8-like negative tone photoresist for MEMS applications by chemical modification", *Proc. SPIE*, Vol.4345, 502 (2001), pp.502-510

[92] J. Liu, B. Cai, J. Zhu, and G. Ding et al., "Process research of high aspect ratio microstructure using SU-8 resist", *Microsystem Technologies*,Vol.10, No.4, May 2005, pp.265-268

[93] Z. Zhou, Q. Huang, and W. Li et al., "The Swelling Effects during the Development Processes of Deep UV Lithography of SU-8 Photoresists: Theoretical Study, Simulation and Verification", *IEEE conference proc. sensor 2007*, Oct 2007, pp.325 – 328

[94] X. Tian, G. Liu, and Y. Tian et al., "Simulation of deep UV lithography with SU-8 resist by using 365 nm light source", *Microsystem Technologies*,Vol.11, No.4-5, April 2005, pp.265-270

[95] C.H. Lin, G.B. Lee, and B.W. Chang et al., "A new fabrication process for ultra-thick microfluidic microstructures utilizing SU-8 photoresist", *Journal of Micromechanics and Microengineering*, Vol.12, Issue 5, pp.590-597, 2002

I

II

III

IV